Ocean-color optical property data derived from the Japanese Ocean Color and Temperature Scanner and the French Polarization and Directionality of the Earth's Reflectances: a comparison study

Menghua Wang, Alice Isaacman, Bryan A. Franz, and Charles R. McClain

We describe our efforts to study and compare the ocean-color data derived from the Japanese Ocean Color and Temperature Scanner (OCTS) and the French Polarization and Directionality of the Earth's Reflectances (POLDER). OCTS and POLDER were both on board Japan's Sun-synchronous Advanced Earth Observing Satellite from August 1996 to June 1997, collecting approximately 10 months of global ocean-color data. This operation provided a unique opportunity for the development of methods and strategies for the merging of ocean-color data from multiple ocean-color sensors. We describe our approach to the development of consistent data-processing algorithms for both OCTS and POLDER and the use of a common *in situ* data set to calibrate vicariously the two sensors. Therefore the OCTS- and POLDER-measured radiances are bridged effectively through common *in situ* measurements. With this approach to the processing of data from two different sensors, the only differences in the derived products from OCTS and POLDER are the differences that are inherited from the instrument characteristics. Results show that there are no obvious bias differences between the OCTS- and POLDER-derived ocean-color products, whereas the differences due to noise, which stem from variations in sensor characteristics, are difficult to correct at the pixel level. The ocean-color data from OCTS and POLDER therefore can be compared and merged in the sense that there is no significant bias between two.

OCIS codes: 010.0010, 280.0280, 010.4450.

1. Introduction

The Japanese Ocean Color and Temperature Scanner (OCTS)[1] and French Polarization and Directionality of the Earth's Reflectances (POLDER)[2] were both flown on the Japanese Sun-synchronous Advanced Earth Observing Satellite (ADEOS) from August 1996 to June 1997, collecting about 10 months of global ocean color data. ADEOS was on a polar orbit at an altitude of 800 km with local crossing time (descending node) at around 10:40 am. This was the first time in history that two ocean-color sensors were on board the same platform and viewed the global ocean with the same temporal and similar global spatial coverages. Therefore the operation provides an ideal case for studying and comparing ocean-color data that is derived from two different sensors, hence allowing the development of a strategy for a ocean-color data merger from multiple ocean-color sensors. The primary goal of the National Aeronautics and Space Administration Sensor Intercomparison and Merger for Biological and Interdisciplinary Oceanic Studies (SIMBIOS) project is to develop methods for the meaningful comparison and merging of data products from multiple ocean-color missions.[3] In a recent study, Wang and Franz[4] show that, using a vicarious intercalibration approach between the modular optoelectronic scanner (MOS)[5] and the Sea-viewing Wide Field-of-View Sensor (SeaWiFS)[6,7] (SeaWiFS ocean color data were used as "truth"), one can meaningfully compare the ocean optical property data derived from two sensors. The bias differences

M. Wang (wang@simbios.gsfc.nasa.gov), A. Isaacman, B. A. Franz, and C. R. McClain are with the National Aeronautics and Space Administration Goddard Space Flight Center, Greenbelt, Maryland 20771. M. Wang is also with the University of Maryland—Baltimore County, Baltimore, Maryland 21210. A Isaacman and B. A. Franz are also with the Science Applications International Corporation General Sciences Corporation, Beltsville, Maryland 20705.

Received 7 March 2001; revised manuscript received 19 September 2001.

0003-6935/02/060974-17$15.00/0

are reduced significantly between the two products. In the Wang–Franz study,[4] measurements from the two sensors had a temporal difference of about 90 min. In this paper, we compare the ocean-color data derived from OCTS and POLDER measurements using consistent data-processing algorithms for both sensors and vicarious calibrations based on a common *in situ* data set from the Marine Optical Bouy (MOBY)[8] in the waters off Hawaii. Therefore differences in the derived ocean-color products from OCTS and POLDER are associated primarily with differences in instrument characteristics. We first give a brief overview of the sensor characteristics of the OCTS and the POLDER and their differences. Detailed algorithm descriptions for processing OCTS and POLDER data are then presented. Next we outline the vicarious calibration scheme in which the OCTS- and POLDER-measured radiances are calibrated with a common *in situ* MOBY data set. Finally, we provide results that compare OCTS and POLDER ocean-color data with global *in situ* measurements and compare a series of OCTS measurements with those of POLDER over the Sargasso Sea and the Bermuda area.

2. Instrument Characterizations

OCTS, which was built and operated by the National Space Development Agency (NASDA) of Japan, is an optical radiometer[1] with a scanning swath of 1400 km and a spatial resolution at nadir of 0.7 km. OCTS has eight spectral bands (out of 12) for ocean-color measurement centered at wavelengths 412, 443, 490, 520, 565, 670, 765, and 865 nm. The bandwidths of the first six bands are 20 nm, and those of the last two near-infrared (NIR) bands are 40 nm. The NIR bands can be used for the atmospheric corrections.[9–11] In addition, OCTS has the capability to tilt operationally the sensor $\pm 20°$ away from nadir to minimize sun-glint contamination. In comparison, POLDER, which was built and operated by the Centre National d'Etudes Spatiales (CNES) of France, is a multiangle imaging radiometer and polarimeter with a 242×274 CCD pushbroom matrix array.[2] POLDER has a wide field of view (2400 km), a spatial resolution at nadir of approximately 6–7 km, and six spectral bands centered at 443, 490, 565, 670, 765, and 865 nm for ocean-color measurement. The bandwidths of the first four visible bands are 20 nm, and those of the two NIR bands are 40 nm. Both 670- and 865-nm bands are designed to measure the polarized radiance, in addition to another 443-nm polarized band. For a given Earth ground scene (target), POLDER can provide up to 14 nearcontemporaneous measurements at various viewing directions; therefore it is useful for deriving atmosphere and/or ground bidirectional reflectance distribution functions. Obviously, these two sensors have many different design characteristics, even though their main goal of retrieving the global ocean-color products is the same. For that purpose, they have six common spectral bands at 443, 490, 565, 670, 765, and 865 nm.

3. Algorithm Descriptions

The data-processing algorithms used for OCTS and POLDER are described in the following two sections. The processing algorithms are implemented in the Multi-Sensor Level-1 to Level-2 (MSL12) software which is freely distributed as part of SeaWiFS Data Analysis System (SeaDAS) software package.[12]

A. Data Processed to Level-1B

The OCTS and POLDER Level-1B data are usually obtained from Japan's NASDA and the French CNES data centers. However, during the ADEOS mission lifetime, approximately 450 GB of real-time OCTS data were collected by the SeaWiFS project through the National Oceanic and Atmospheric Administration ground stations at Wallops, Virginia and Fairbanks, Alaska. Since standard OCTS Level-0 to Level-1B software was not available publicly, the SIMBIOS project was engaged in the development and enhancement of the Level-0 to Level-1B processing software, with specific attention given to the improvement of geolocation and image registration. Herein, we briefly describe the OCTS Level-0 to Level-1B processing software developed by the SIMBIOS project.

In general, the processing of Level-0 data to Level-1B includes the conversion of raw sensor counts to physical units and the assignment of geolocation information to each observation (pixel, detector, and band). Several factors in the design of the OCTS instrument complicate this process. Each OCTS band is divided into 10 individual detectors, where each detector is associated with a separate scan line. Each detector has a slightly different and apparently nonlinear responsivity, which gives rise to horizontal striping in the OCTS imagery.[13] The basis for the SIMBIOS calibration is the NASDA Version 3 preflight calibration and relative detector calibration.[14] The relative detector calibration substantially reduces the striping effects, but low-level artifacts are still visible, and they can become significant following the removal of the large, comparatively smooth atmospheric signal.

The design of the OCTS scan mirror and focal plane results in a severe misalignment of the line of sight for different spectral bands that radiances are measured at essentially the same time.[13] To perform atmospheric correction and derive chlorophyll concentration at a given location, we must coregister the bands to that location. The SIMBIOS project developed a registration technique in which an idealized focal-plane geometry is defined, and all bands are resampled by use of a nearest-neighbor approach to match the idealized ground track. This method is similar in concept to the approach of using OCTS band 1 as a nearest-neighbor matching target,[13] but the idealized focal-plane geometry also eliminates scan-to-scan overlap. While this coregistration process can correct for differences in geolocation between bands, the resampled observations come from different lines of sight with unique sensor-to-ground and

sun-to-ground geometries. To ensure accurate atmospheric correction, we save the true solar and sensor viewing angles for each band in the Level-1B file for use in the Level-1B to Level-2 processing. Note that this is not possible with NASDA standard Level-1B products, because only nominal angles are saved.

Before the registration process can begin, the observations from each band must be navigated accurately. The geolocation algorithm used for SIMBIOS OCTS processing is a modified version of the method used for SeaWiFS navigation.[15] This technique has the potential to yield an exact solution to the geolocation of each scan line when the spacecraft position and sensor geometry are accurately known. To improve geolocation accuracy, the SIMBIOS project derived time-dependent attitude and tilt adjustments using an automated navigation-assessment technique that was based on island targets.[16] Results show that, with the SIMBIOS Level-1B data processing, the OCTS navigation is accurate to approximately 1 km.

The OCTS Level-1B data processed with the SIMBIOS code usually agree well with the NASDA standard Level-1B product. For OCTS bands 1–8, the radiance-frequency distributions from the two processes are nearly identical. However, the radiance differences based on a pixel by pixel comparison can disagree owing to small differences in navigation and band coregistration, i.e., in such comparisons, the corresponding pixels from the NASDA standard Level-1B and the SIMBIOS Level-0 to Level-1B routine are usually not the same. In a typical example, differences in terms of radiance were found to be 0.54%, 0.53%, 0.54%, 0.85%, 1.00%, 1.62%, 2.20%, and 2.67% for bands 1–8, respectively.

B. Data Processed from Level-1B to Level-2

For ocean-color remote sensing, Level-1B to Level-2 data processing mainly involves the atmospheric correction,[9–11,17,18] in which the radiance contributions from the atmosphere and ocean surface as well as their interactions are removed from the sensor-measured signals at the top of the atmosphere. The radiance contributions from the ocean, i.e., the normalized water-leaving radiances just above the sea surface, can then be retrieved. Herein, the normalized water-leaving radiance $[L_w(\lambda)]_N$ is defined as

$$[L_w(\lambda)]_N = L_w(\lambda)/[\cos\,\theta_0 t_0(\lambda)], \qquad (1)$$

where $L_w(\lambda)$ is the water-leaving radiance just above the surface and $t_0(\lambda)$ is the atmospheric diffuse transmittance[19,20] in the solar direction with the solar zenith angle of θ_0. A simple empirical algorithm[21–23] can then be used to derive the ocean chlorophyll concentration from the normalized water-leaving radiances. In the following, a consistent atmospheric-correction algorithm applied to OCTS and POLDER as well as a bio-optical algorithm tuned to OCTS and POLDER spectral bands are briefly described. The data-processing procedures, in particular for POLDER, are outlined.

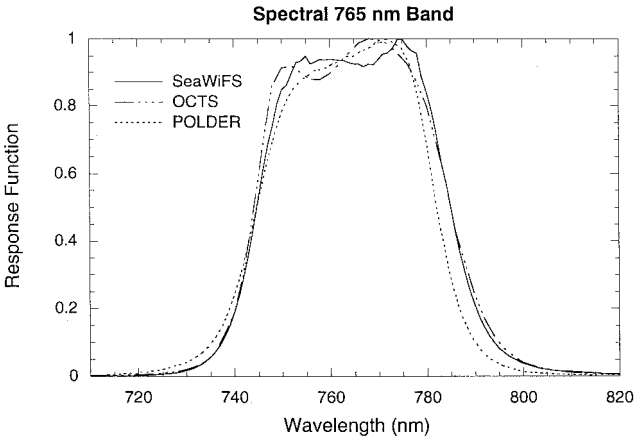

Fig. 1. The OCTS and POLDER 765-nm band spectral response functions compared with that of SeaWiFS.

1. *Atmospheric Corrections*

Based on a study by Wang,[24] the SIMBIOS project has developed the MSL12 software for processing data from multiple ocean-color sensors. MSL12 is an implementation of the standard SeaWiFS atmospheric-correction algorithm,[9,17] with some generalizations to allow for application to OCTS, POLDER, and other ocean-color sensors (e.g., MOS).[4,24] Therefore a consistent atmospheric-correction algorithm can be used to process data from OCTS and POLDER.

Similar to SeaWiFS, both OCTS and POLDER have two NIR bands at 765 and 865 nm for the atmospheric correction. However, the 765-nm spectral band completely encompasses the oxygen A-band absorption. Figure 1 compares the OCTS and POLDER 765-nm band spectral response functions (SRF) with that of SeaWiFS. Clearly, both OCTS and POLDER 765-nm band SRFs are almost identical to that of SeaWiFS. Therefore the same SeaWiFS oxygen A-band absorption-correction algorithm[25] can be used for both OCTS and POLDER. A small difference in the SRFs (mainly between POLDER and SeaWiFS) is within the uncertainty of the correction algorithm.[25,26]

There are some major improvements in MSL12 for the OCTS and POLDER data processing that are concurrent with changes in processing algorithms for the SeaWiFS third data reprocessing in May 2000.[27] Some specific atmospheric-correction algorithm improvements include

1. An iterative correction algorithm that accounts for the ocean radiance contributions at two NIR wavelengths (765 and 865 nm), was developed and implemented in the data processing.[28]
2. An improved Rayleigh radiance lookup table, in which the Rayleigh (air molecules) scattering radiance is a function of the sea-surface wind speed (in addition to solar and sensor viewing geometry and

wavelength dependence),[29] was generated and implemented in the MSL12 data-processing system[30] for OCTS and POLDER.

3. A sun-glint contamination correction algorithm, which effectively removes the sun-glint residual contamination radiance around the subsolar point, was developed and implemented in MSL12.[31]

4. Correction of the ocean whitecap radiance contributions[17] was updated[27] using some current *in situ* measurements.[32–34]

5. The current 12 aerosol models used in the generation of aerosol lookup tables for the atmospheric correction are Oceanic with relative humidity (RH) of 99%, Maritime with RH of 50%, 70%, 90%, and 99%, Coastal with RH of 50%, 70%, 90%, and 99%, and Tropospheric with RH of 50%, 90%, and 99%.[27] The Oceanic, Maritime, and Tropospheric models are from Shettle and Fenn,[35] whereas the Coastal model was derived using data from the Shettle and Fenn models.[9]

6. A correction algorithm for the sensor spectral bandpass effects on the derived normalized water-leaving radiances for SeaWiFS[36] was developed. The correction procedure converts the sensor spectral bandpass-weighted normalized water-leaving radiances to the values at their nominal center wavelengths.[36] Similar algorithms for both OCTS and POLDER were also implemented in MSL12. Similar to Wang *et al.*[36] [presented in Fig. 3(b) of Ref. 36], Fig. 2(a) and 2(b) provide the spectral bandpass correction factor $r(\lambda)$ as a function of the sensor-derived (uncorrected) ratio values between the normalized water-leaving radiances at wavelengths 490 and 565 nm. Note that $r(\lambda) > 1$ indicates underestimation of the derived normalized water-leaving radiance, whereas $r(\lambda) < 1$ indicates overestimation. Figure 2(a) shows the correction factors for the OCTSs spectral bands, while Fig. 2(b) shows those for POLDER. Figure 2(a) shows that, without corrections, the OCTS-derived $[L_w(\lambda)]_N$ at 565 nm is underestimated (~8%), while the values at 520 nm are overestimated (up to ~17%) for clear ocean waters. Other OCTS bands (412, 443, and 490 nm) have almost no spectral bandpass effects. On the other hand, without corrections, the POLDER 490 nm band has ~5% underestimation for the derived value in clear ocean waters, while for the 565-nm band there is underestimation from about 3.5–1.5% of the derived values for ocean waters ranging from productive to nonproductive (clear) cases. Clearly, corrections of the sensor spectral bandpass effects are necessary in order to have a meaningful Level 2 product comparison derived from two different sensors, e.g., OCTS and POLDER.

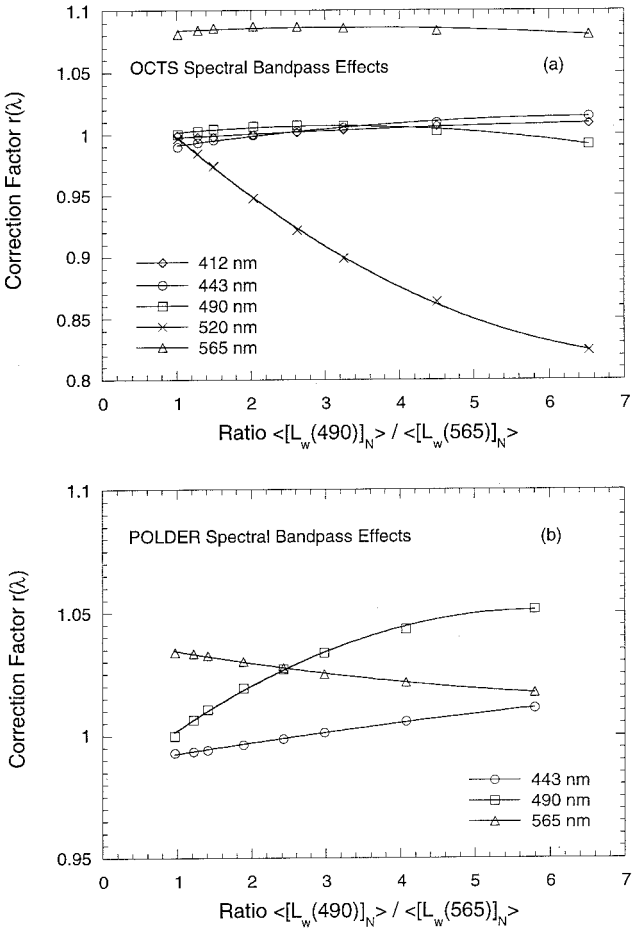

Fig. 2. Spectral bandpass correction factor $r(\lambda)$ as a function of the sensor-derived two-band ratio values in the normalized water-leaving radiances between wavelengths 490 and 565 nm for (a) the OCTS bands 412, 443, 490, 520, and 565 nm and (b) the POLDER bands 443, 490, and 565 nm. The curves are the least-squares fit.

2. *Bio-Optical Algorithms*

In this study, we use the bio-optical algorithm of ocean chlorophyll 2 (Ref. 23) for deriving the ocean chlorophyll concentration from the sensor-retrieved normalized water-leaving radiance $[L_w(\lambda)]_N$. Therefore a consistent bio-optical algorithm is used in deriving chlorophyll concentration for both OCTS and POLDER. The OC2 algorithm was modified to account for the effects of the spectral band differences between the OCTS and POLDER 565-nm band and the SeaWiFS 555-nm band, i.e.,

$$\mathrm{Chl} = 10^{(0.3164 - 2.132R + 0.6303R^2 + 0.004R^3)} - 0.0708, \quad (2)$$

where *Chl* is the chlorophyll-a concentration in (mg m^{-3}) and

$$R = [\rho_w(490)]_N / [\rho_w(565)]_N \quad (3)$$

is the ratio between the normalized water-leaving reflectances at 490 and 565 nm. The normalized water-leaving reflectance, $[\rho_w(\lambda)]_N$, is defined as

$$[\rho_w(\lambda)]_N = \pi [L_w(\lambda)]_N / F_0(\lambda), \quad (4)$$

where $[L_w(\lambda)]_N$ is the sensor-derived normalized water-leaving radiance and $F_0(\lambda)$ is the extraterrestrial solar irradiance.

3. A Specific Data-Processing Procedure for POLDER

As we discussed in previous sections, for a given location (scene), POLDER can acquire as many as 14 near-contemporaneous measurements. Therefore up to 14 values of the Level 2 product for the same ocean scene can be derived. However, it was noted that, for a given scene, the POLDER-derived products, e.g., normalized water-leaving radiances, often have high variations (up to 1 order of magnitude) between various POLDER viewing directions. These variations are possibly related to the POLDER subpixel cloud contamination and/or band nonlinear responses.[37] It was also found that, for a given scene, there was no obvious correlation between the POLDER-derived $[L_w(\lambda)]_N$ and its viewing direction (angle). Therefore we used an averaging scheme to eliminate points with high variation and to reduce data noise in the derived product. First, for a given pixel, the derived normalized water-leaving radiances from all possible POLDER viewing directions were averaged. Data points that were within 50% variation of the first averaged value (i.e., 0.5–1.5 of average value) were then used to derive the final mean value and considered as the POLDER-derived normalized water-leaving radiances for the pixel. This averaging scheme was used in deriving the POLDER vicarious gain coefficients, as well as the POLDER Level 2 products.

4. Vicarious Calibrations with the Marine Optical Buoy in situ Measurements

It is well known that, for ocean-color remote sensing, an on-orbit vicarious calibration of sensor and algorithms is necessary.[38] Vicarious calibration techniques have been successfully applied to SeaWiFS[39,40] and also used to intercalibrate MOS and SeaWiFS data.[4] In this study, a vicarious calibration for OCTS and POLDER using the *in situ* measurements from the MOBY[8] was carried out. The sensor vicarious gain coefficients, $G^{(VC)}(\lambda)$, are defined through

$$L_t^{(VC)}(\lambda) = G^{(VC)}(\lambda) L_t^{(\mathrm{meas})}(\lambda), \tag{5}$$

where $L_t^{(\mathrm{meas})}(\lambda)$ is sensor-measured Level-1B radiance from OCTS and POLDER and $L_t^{(VC)}(\lambda)$ is the vicariously calibrated radiance that is used in the Level-1B to Level-2 algorithms as the correct value of $L_t(\lambda)$. The vicarious calibration procedure was performed as follows. First, for the 865-nm band, it was assumed that gain coefficients were not changed. They were equivalent to the values suggested by NASDA and CNES. The in-flight gains for the OCTS and POLDER 865-nm bands were derived by NASDA and CNES as 0.89 and 1.05, respectively.[14,41] Next, we derived the gain coefficient of the 765-nm band by forcing the atmospheric-correction algorithm to select a maritime aerosol type over the MOBY site. The procedure was similar to the methods used in the adjustment of the SeaWiFS 765-nm band.[39] Finally, with the derived 765-nm gain coefficient, the MOBY *in situ* measurements were used to calibrate the visible bands,[40] i.e., the OCTS and POLDER visible bands were calibrated such that, with the atmospheric corrections, the derived normalized water-leaving radiances were equivalent to the MOBY *in situ* measurements.

Table 1. Derived Vicarious Gain Coefficients for OCTS and POLDER Spectral

Wavelength (nm)	Gain Coefficient $G^{(VC)}(\lambda)$	
	OCTS	POLDER
412	1.12426	–
443	1.01539	1.06465
490	0.95084	1.02350
520	1.01784	–
565	1.03255	0.97541
670	1.00859	1.01845
765	0.92093	1.02946
865	1.00000	1.00000

The location of the MOBY site is usually in stable clear-ocean waters, and the aerosols are predominantly marine. The MOBY program has been providing consistently high-quality clear-ocean optical data since 1997. Unfortunately, there were some problems with the early deployment of MOBY in 1996, limiting the number of usable calibration samples to five measurements spanning the period of November 1996–February 1997. Specifically, five *in situ* measurements that were taken on November 26, 1996 and January 13, January 17, February 16, and February 23, 1997 were used. Table 1 provides the derived gain coefficients for the OCTS and POLDER spectral bands.

5. Results

Using the derived vicarious gain coefficients, we processed OCTS and POLDER data to Level-2 products from either OCTS Level-0 (data acquired from Wallops, Virginia) and/or OCTS Level-1B data and POLDER Level-1B data using MSL12. As discussed in the previous sections, the processing algorithms for both OCTS and POLDER are essentially the same as for SeaWiFS, although some specific modifications are necessary, depending on sensor characteristics. In the following four sections, we provide OCTS and POLDER matchup analyses that compare satellite retrievals with *in situ* measurements, ocean-color data comparisons between the two sensors, and some data analyses and discussions.

A. Global in situ $[L_w(\lambda)]_N$ Matchup Analyses

An extensive set of *in situ* data taken during the time of the OCTS and POLDER missions was archived in the SeaWiFS Bio-optical Archive and Storage System (SeaBASS) database. These *in situ* data, which were used for the OCTS and POLDER matchup analyses, were acquired mainly from five regions: the California Current (35 °N and 121 °W), the Gulf of California (26 °N and 110 °W), the MOBY site (21 °N and 157 °W), the Labrador Sea (57 °N and 53 °W),

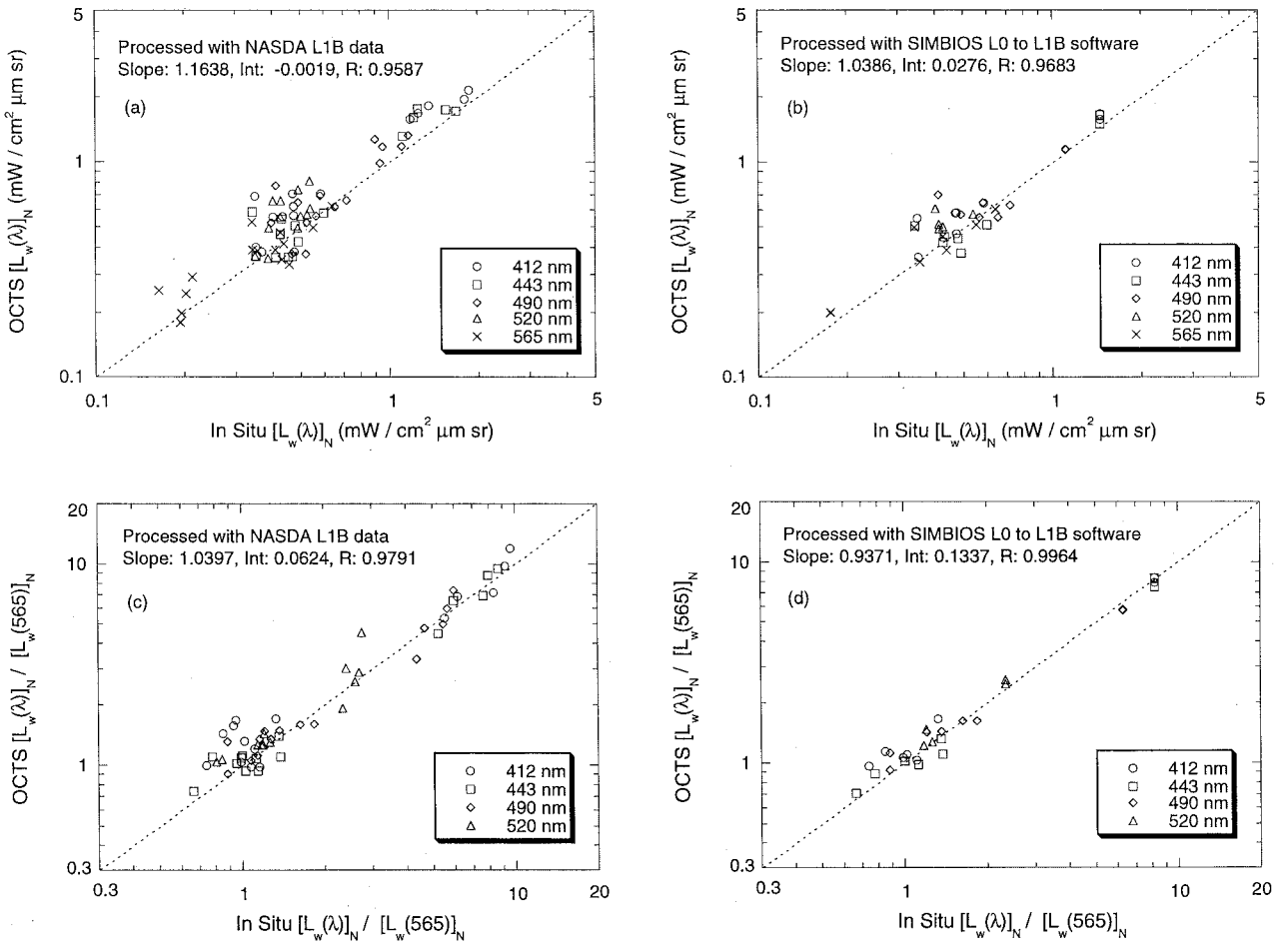

Fig. 3. OCTS-derived ocean-color parameters compared with the *in situ* measurements for (a) $[L_w(\lambda)]_N$ with OCTS NASDA Level-1B data; (b) $[L_w(\lambda)]_N$ with OCTS Wallops Level-0 data; (c) ratio $[L_w(\lambda)]_N/[L_w(565)]_N$ with OCTS NASDA Level-1B data; and (d) ratio $[L_w(\lambda)]_N/[L_w(565)]_N$ with OCTS Wallops Level-0 data. Each plot indicates linear fit coefficients of slope, intercept (Int), and the correlation coefficient (R).

and the Bermuda area (32 °N and 64 °W). Note that, for the *in situ* data around the MOBY site, only those data that were not used for the vicarious calibration were used. In the matchup comparison analyses, the satellite and *in situ* data were screened and obtained through the following procedure: (i) the differences of time and solar zenith angle between satellite and *in situ* measurements were less than 4 hours and 15°, respectively; (ii) the solar zenith angle and sensor-viewing angle for OCTS and POLDER were $\leq$60°; (iii) the *in situ* measurement was between 9 am and 3 pm local time; (iv) in the matchup analyses, the OCTS $[L_w(\lambda)]_N$ was derived by averaging data in a 5-km circle centered at the location of the *in situ* measurement, and only data for which a coefficient of determination (the ratio of standard deviation to average) was less than 0.5 were considered; and (v) as discussed previously, we derived POLDER results by first averaging over all possible viewing directions (up to 14 values) and then reaveraging data after eliminating data points whose differences compared with the first averaged value were $>\pm$50%.

Figures 3 and 4 provide matchup results for the OCTS and POLDER compared with the *in situ* measurements. Figures 3(a) and 3(b) show matchup results for the normalized water-leaving radiance $[L_w(\lambda)]_N$ derived from OCTS NASDA standard Level-1B data and Wallops Level-0 data (using SIMBIOS Level-0 to Level-1B processing), respectively. Figure 4(a) shows the matchup results derived from POLDER CNES Level-1B data compared with the *in situ* measurements. Note that the number of the *in situ* data used in Figs. 3(a), 3(b), and 4(a) is 15, 8, and 22, respectively. There are four duplicated *in situ* data used in Figs. 3(a) and 3(b). Therefore, the number of *in situ* data used for the OCTS and POLDER matchup analyses was slightly different. This is because of different viewing geometry between two sensors, e.g., OCTS could view the sun glint and/or clouds (such pixels are masked out), while some of POLDER's multiangle measurements are possibly not contaminated, and also because of some differences in their data-screening procedures for matchup analyses. Figures 3(c) and 3(d) compare the OCTS derived two-band ratio value $[L_w(\lambda)]_N/[L_w(565)]_N$ from NASDA Level-1B and Wallops Level-0 data, re-

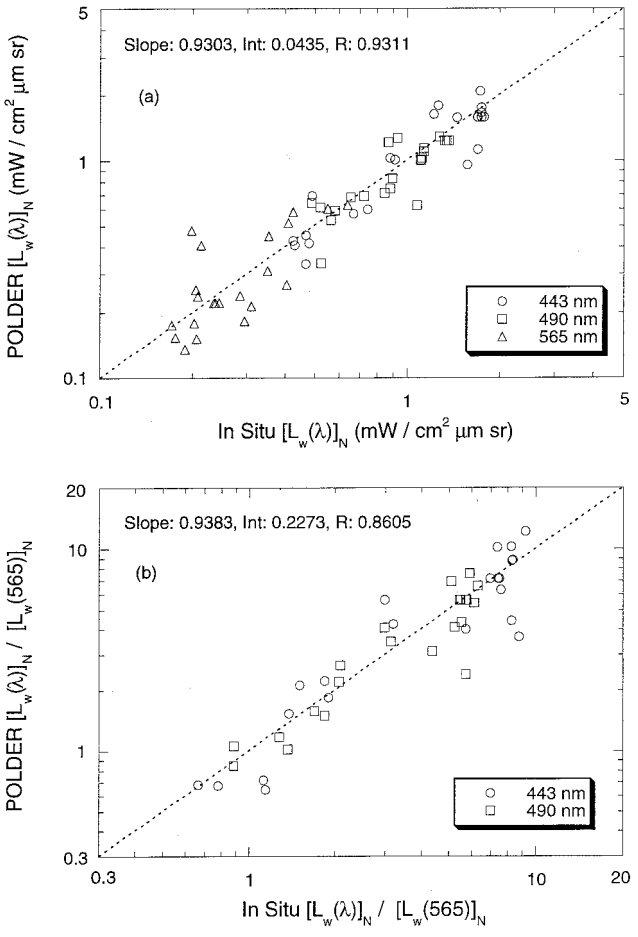

Fig. 4. POLDER-derived ocean-color parameters compared with the *in situ* measurements from POLDER CNES Level-1B data for (a) $[L_w(\lambda)]_N$ and (b) ratio $[L_w(\lambda)]_N/[L_w(565)]_N$ values. Each plot indicates linear fit coefficients of slope, intercept (Int), and the correlation coefficient (R).

spectively, with results from *in situ* measurements, while Fig. 4(b) shows the same results from POLDER matchup comparisons. The matchup analyses for the two-band ratio value in the derived $[L_w(\lambda)]_N$ are useful, since they are inputs for the ocean-color bio-optical algorithms.[21–23]

Results in Figs. 3 and 4 show that, after vicarious calibration using the MOBY data, the derived $[L_w(\lambda)]_N$ and $[L_w(\lambda)]_N/[L_w(565)]_N$ from the OCTS and POLDER measurements compared reasonably well with the *in situ* data. Note that each plot gives the linear fit showing coefficients of slope, intercept (Int), and the correlation coefficient (R). (A perfect match would have slope of 1, an intercept of 0, and a correlation coefficient of 1). It appears, however, that the OCTS-derived $[L_w(\lambda)]_N$ values were slightly overestimated (slope > 1.0), while the POLDER results were slightly underestimated (slope < 1.0). The derived two-band ratio values $[L_w(\lambda)]_N/[L_w(565)]_N$ compared better with the *in situ* measurements than those of $[L_w(\lambda)]_N$, indicating that the derived ocean chlorophyll concentrations are reasonably accurate. Note that the correlation coefficients derived from the POLDER matchup results are slightly lower than those from the OCTS comparisons.

B. OCTS and POLDER $[L_w(\lambda)]_N$ Comparisons

A series of measurements from OCTS and POLDER over the Sargasso Sea and the Bermuda area were collected for comparison. The satellite observations were obtained from a colocated 3° × 3° box over the Sargasso Sea (latitude of 23.5 °N to 26.5 °N and longitude of 70 °W to 73 °W) and the Bermuda area (latitude of 30 °N to 33 °N and longitude of 62.7 °W to 65.7 °W). Over the Sargasso Sea and the Bermuda area, OCTS data were all collected through the ground station at Wallops, Virginia. Therefore OCTS data were processed from Level-0 to Level-1B with the SIMBIOS code, and then to Level-2 using MSL12. Figures 5 and 6 provide color images for the OCTS- and POLDER-derived $[L_w(\lambda)]_N$ comparisons for wavelengths of 443, 490, and 565 nm over the Sargasso Sea and the Bermuda area. Figure 5 is for the results over the Sargasso Sea, while Fig. 6 is for comparisons over the Bermuda area. The color scales for $[L_w(\lambda)]_N$ images are indicated at the bottom of Fig. 6. $[L_w(\lambda)]_N$ for 443 and 490 nm is scaled from 0 to 3 (mW cm^{-2} μm^{-1} sr^{-1}), while $[L_w(\lambda)]_N$ for 565 nm is scaled from 0 to 0.8 (mW cm^{-2} μm^{-1} sr^{-1}). In Figs. 5 and 6, columns 1–3 are the OCTS-derived $[L_w(\lambda)]_N$ images for 443, 490, and 565 nm, respectively, and columns 4–6 are the POLDER-derived results for 443, 490, and 565 nm, respectively. In addition, at the left side of the images are the dates when OCTS and POLDER measurements were acquired. Over the Sargasso Sea, OCTS and POLDER data were acquired on November 20 and December 19, 1996, and January 26, February 17, March 11, April 14, and May 20, 1997 (there were data from each month for seven months), while data were acquired on December 12, 1996, and March 19, May 3, May 7, and June 10, 1997 over the Bermuda area. In Figs. 5 and 6, each image represents a 3° × 3° box over the Sargasso Sea or the Bermuda area.

Results in Figs. 5 and 6 show a reasonable agreement between OCTS- and POLDER-derived $[L_w(\lambda)]_N$ values. Over the Sargasso Sea, both spatial and temporal variations of ocean color were well captured by both OCTS and POLDER. For example, $[L_w(\lambda)]_N$ values at 443 nm changed from November (note the spatial variations in the November image from both OCTS and POLDER) to a lower value in December and January, then elevated in February, and finally reached their highest values in the spring. The spatial $[L_w(\lambda)]_N$ distributions from OCTS and POLDER are comparable. However, there are some obvious differences, e.g., POLDER has a larger pixel size (low spatial resolution), and it appears that the POLDER results show more noise than results from OCTS. Some sparkling points in the POLDER $[L_w(\lambda)]_N$ images are mostly cloud-edge effects, probably owing to subpixel cloud contamination because of POLDER low-spatial-resolution measurement.

Figures 7 and 8 compare the histogram (%) of the retrieved $[L_w(\lambda)]_N$ between OCTS and POLDER over

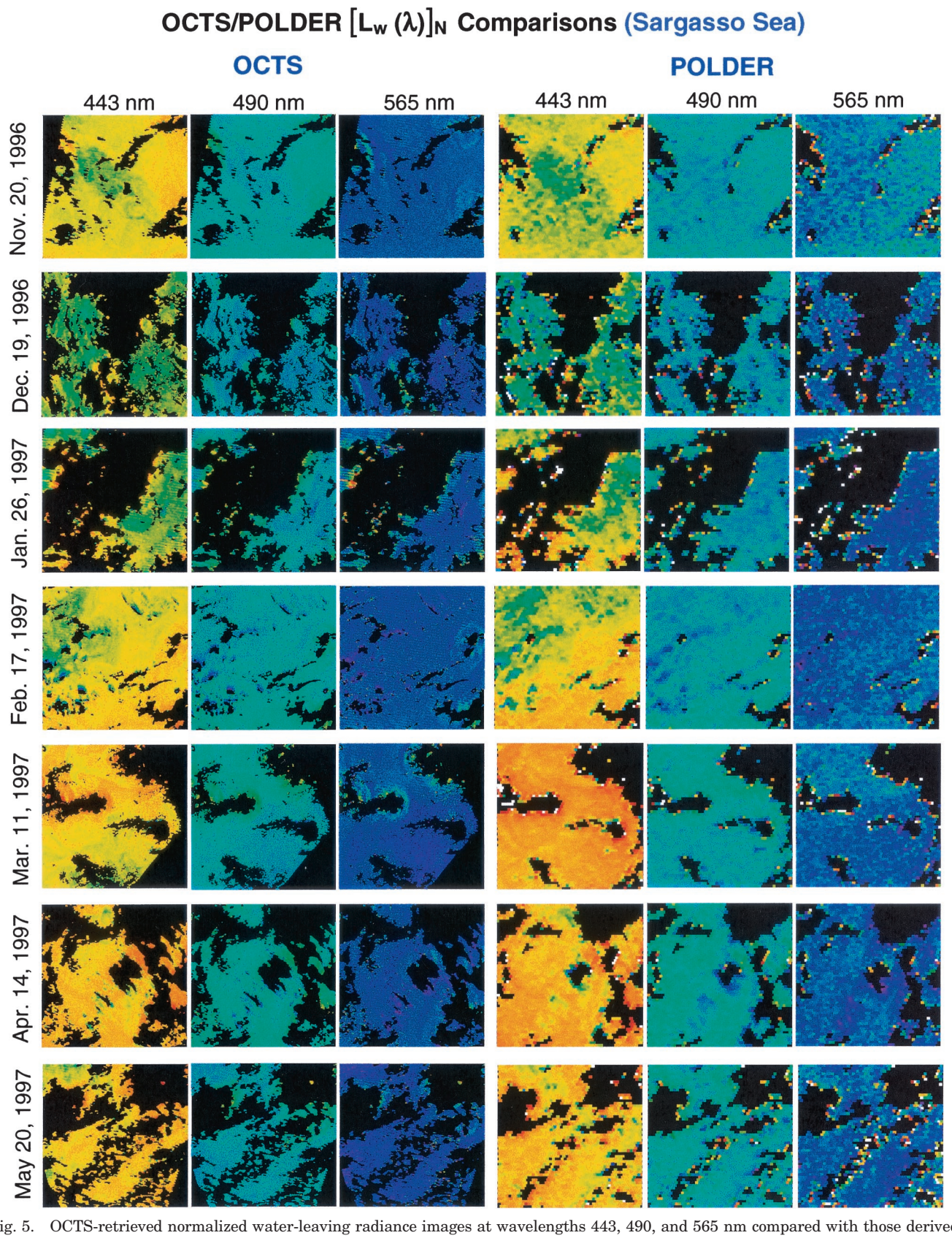

Fig. 5. OCTS-retrieved normalized water-leaving radiance images at wavelengths 443, 490, and 565 nm compared with those derived from POLDER measurements for ocean water over the Sargasso Sea from Nov. 20, 1996 to May 20, 1997. The color scales for $[L_w(\lambda)]_N$ are indicated at the bottom of Fig. 6.

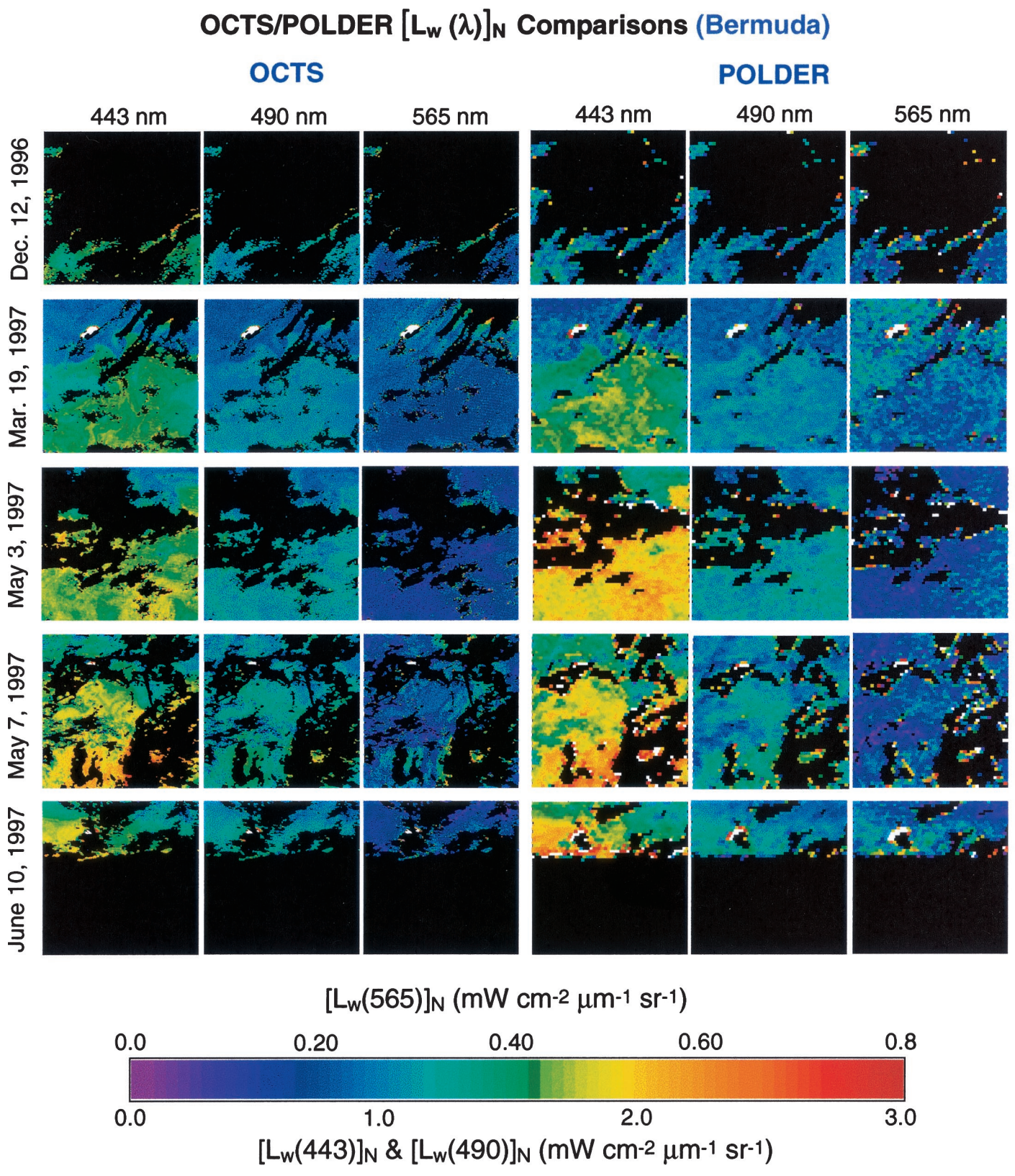

Fig. 6. The OCTS-retrieved normalized water-leaving radiance images at wavelengths 443, 490, and 565 nm compared with those derived from POLDER measurements for ocean water over the Bermuda area from Dec. 12, 1996 to June 10, 1997.

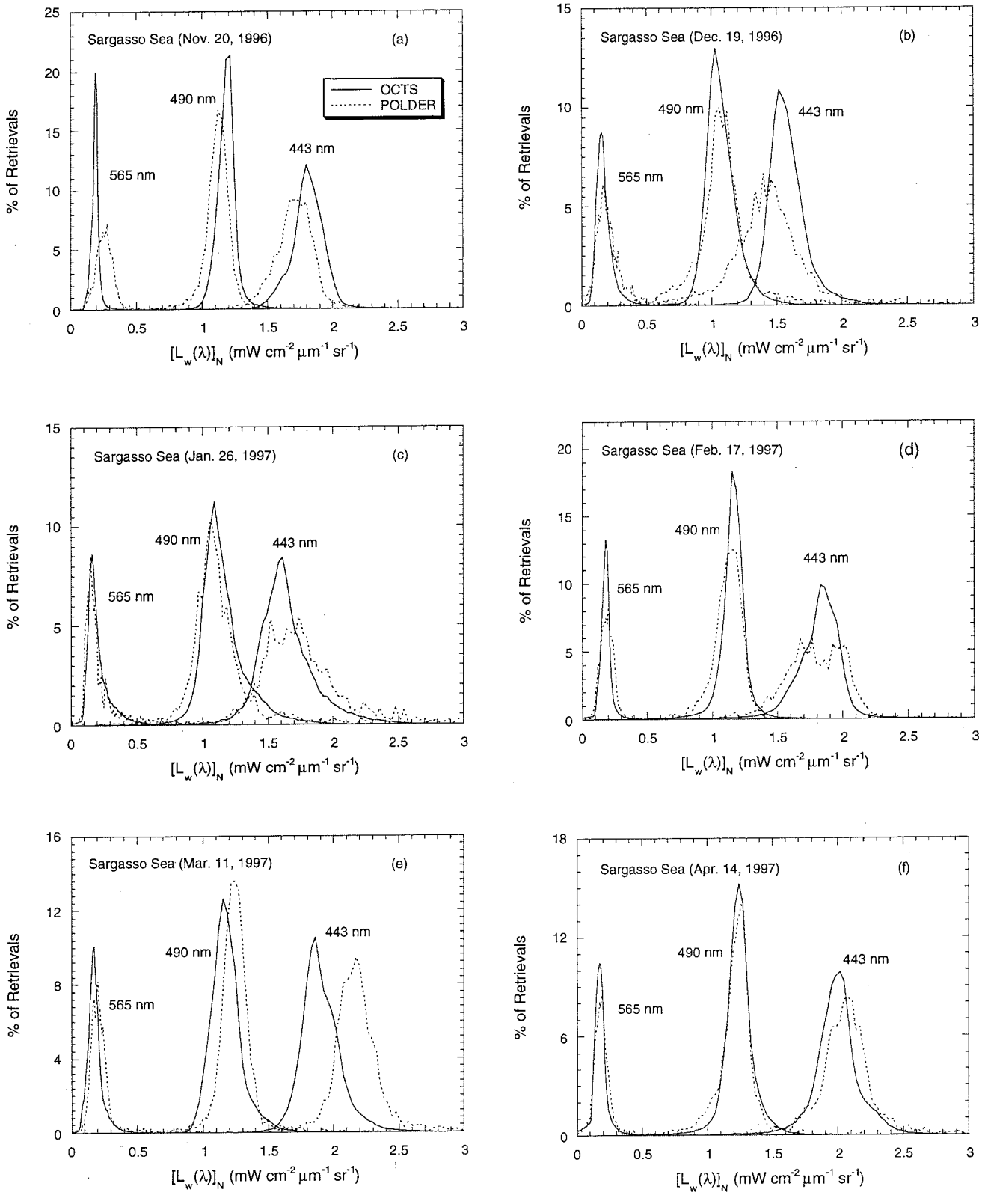

Fig. 7. Histogram (%) of the OCTS-retrieved normalized water-leaving radiances at wavelengths 443, 490, and 565 nm compared with those from POLDER measurements as in Fig. 5 for (a)–(g) over the Sargasso Sea from Nov. 20, 1996 to Apr. 14, 1997.

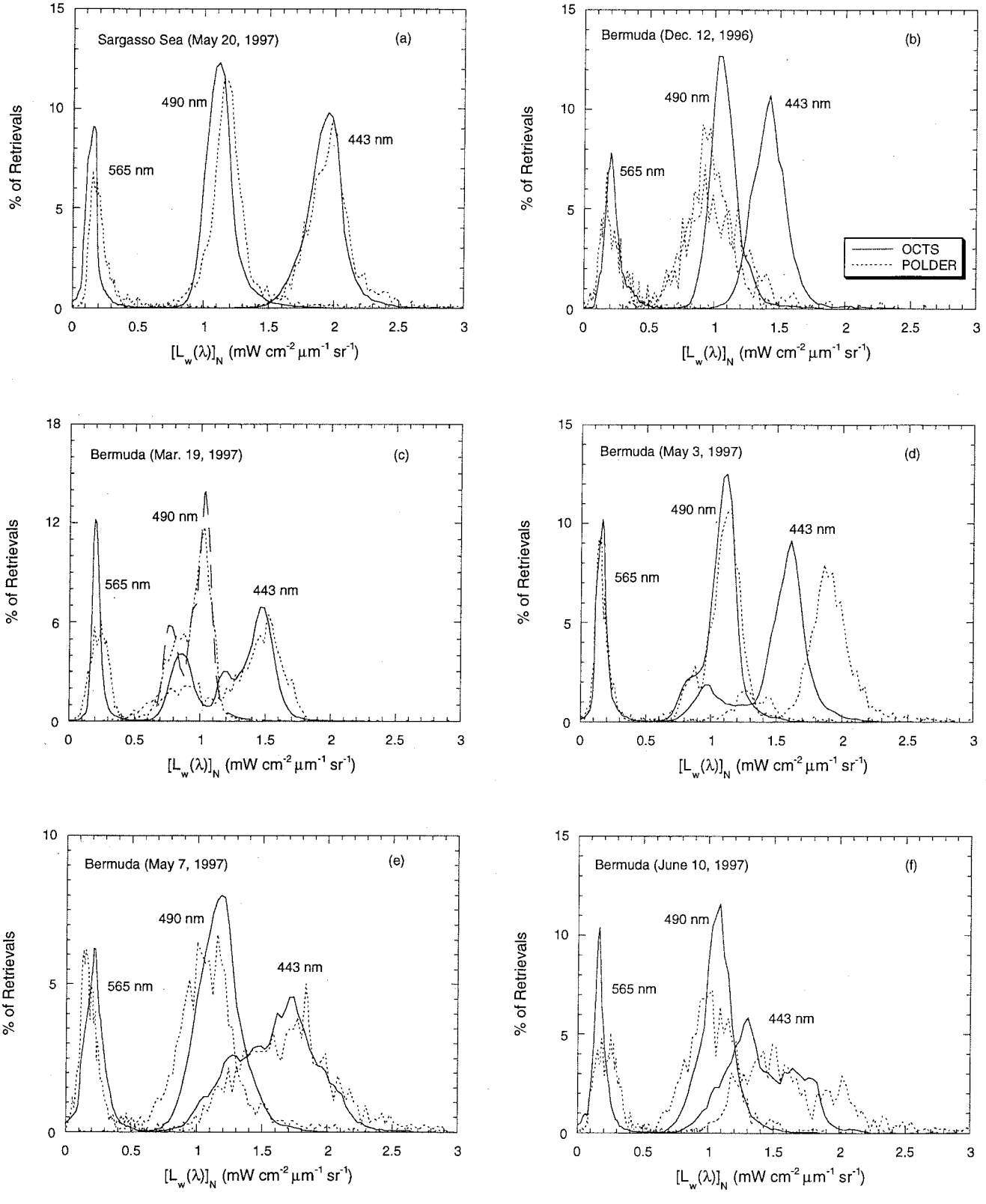

Fig. 8. Histogram (%) of the OCTS-retrieved normalized water-leaving radiances at wavelengths 443, 490, and 565 nm compared with those from POLDER measurements as for (a) the Sargasso Sea on May 20, 1997 and for (b)–(f) the Bermuda area from Dec. 12, 1996 to June 10, 1997.

Table 2. OCTS/POLDER Comparisons in the Retrieved $[L_w(\lambda)]_N$ (Mode Value) over the Sargasso Sea from Nov. 20, 1996 to May 20, 1997

	$[L_w(443)]_N$[a]			$[L_w(490)]_N$[a]			$[L_w(565)]_N$[a]		
Date	OCTS	POLDER	Ratio[b]	OCTS	POLDER	Ratio[b]	OCTS	POLDER	Ratio[b]
Nov. 20, 1996	1.8015	1.7500	1.029	1.2209	1.1503	1.061	0.1975	0.2844	0.694
Dec. 19, 1996	1.5489	1.4115	1.097	1.0491	1.1101	0.945	0.1519	0.1606	0.946
Jan. 26, 1997	1.6381	1.7798	0.920	1.1048	1.0874	1.016	0.1643	0.1587	1.035
Feb. 17, 1997	1.8567	1.7216	1.078	1.1591	1.1659	0.994	0.1841	0.2048	0.899
Mar. 11, 1997	1.8705	2.2018	0.850	1.1722	1.2684	0.924	0.1717	0.2077	0.827
Apr. 14, 1997	2.0278	2.0893	0.971	1.2324	1.2880	0.957	0.1872	0.1877	0.997
May 20, 1997	1.9583	2.0156	0.972	1.1064	1.1901	0.930	0.1576	0.1525	1.033

[a]unit of (mW cm^{-2} μm^{-1} sr^{-1}).
[b]Ratio of the OCTS/POLDER $[L_w(\lambda)]_N$ values.

the Sargasso Sea and the Bermuda area. Figures 7(a)–7(f) and Fig. 8(a) are comparison results for the Sargasso Sea for data acquired from November 20, 1996 to May 20, 1997, while Figs. 8(b)–8(f) are for the Bermuda area for measurements acquired from December 12, 1996 to June 10, 1997. The OCTS and POLDER $[L_w(\lambda)]_N$ at 490 and 565 nm usually compare quite well, with small variations between the two measurements, while the POLDER $[L_w(\lambda)]_N$ at 443 nm shows significant variations compared with the OCTS results (sometimes high and sometimes low). The shape of the histogram distributions from OCTS and POLDER, however, are generally similar. Tables 2 and 3 give quantitative comparisons of the retrieved $[L_w(\lambda)]_N$ between OCTS and POLDER for the mode (peak) values in the histograms, as presented in Figs. 7 and 8. Tables 2 and 3 are results for the Sargasso Sea and the Bermuda area, respectively. Although there are some variations in the derived $[L_w(\lambda)]_N$ values between OCTS and POLDER, the overall average ratio values of OCTS/POLDER for $[L_w(\lambda)]_N$ 443, 490, and 565 nm for all cases (total of 12) in Tables 2 and 3 are: 1.0004, 1.0103, and 0.9840 with standard deviations of 0.1754, 0.0728, and 0.1924. These results indicate that, with our approach in processing OCTS and POLDER data, there are no obvious bias differences in the derived $[L_w(\lambda)]_N$ between the two sensors, whereas the noise differences are difficult to correct since they depend mainly on the sensor characteristics.

C. OCTS and POLDER Chlorophyll-a Comparisons

Figures 9 and 10 provide comparisons of chlorophyll-a concentration derived from OCTS and POLDER using the ocean chlorophyll 2 algorithm,[23] which was modified for OCTS and POLDER, over the Sargasso Sea and the Bermuda area. Figure 9 shows results for the Sargasso sea, while Fig. 10 shows those of the Bermuda area. The color images are scaled logarithmically from 0.01 to 5 (mg m^{-3}), and the color scale is indicated at the bottom of Fig. 10. In Figs. 9 and 10, columns 1 and 2 are color images, respectively, for the OCTS- and POLDER-derived chlorophyll-a concentrations, while column 3 shows a histogram comparison of the distributions between the two color images.

Over the Bermuda area (Fig. 10), there were some *in situ* measurements that were acquired at about the same time as for some of the OCTS and POLDER measurements. These data are archived in the SeaBASS data base. The *in situ* data were taken near the center of the Bermuda 3° × 3° box area (center of the images). These *in situ* data are shown as vertical bars in the histograms in Fig. 10. Therefore for the case of December 12, 1996, the OCTS- and POLDER-derived chlorophyll values appear to be underestimated, as compared with the *in situ* data. However, there were no retrievals from OCTS and POLDER over the center and top-most two-thirds part of the image box area. Therefore the satellite values may not be representative for comparison with

Table 3. OCTS/POLDER Comparisons in the Retrieved $[L_w(\lambda)]_N$ (Mode Value) over the Bermuda Area from Dec. 12, 1996 to June 10, 1997

	$[L_w(443)]_N$[a]			$[L_w(490)]_N$[a]			$[L_w(565)]_N$[a]		
Date	OCTS	POLDER	Ratio[b]	OCTS	POLDER	Ratio[b]	OCTS	POLDER	Ratio[b]
Dec. 12, 1996	1.4346	0.9627	1.490	1.0865	0.9672	1.123	0.2093	0.1777	1.178
Mar. 19, 1997	1.4925	1.5656	0.953	1.0410	1.0329	1.008	0.2104	0.2530	0.832
May 3, 1997	1.6149	1.9393	0.833	1.1171	1.1603	0.963	0.1616	0.1414	1.143
May 7, 1997	1.7566	1.8485	0.950	1.1937	1.0473	1.140	0.2121	0.1515	1.400
June 10, 1997	1.3194	1.5309	0.862	1.1024	1.0383	1.062	0.1575	0.1911	0.824

[a]unit of (mW cm^{-2} μm^{-1} sr^{-1}).
[b]Ratio of the OCTS/POLDER $[L_w(\lambda)]_N$ values.

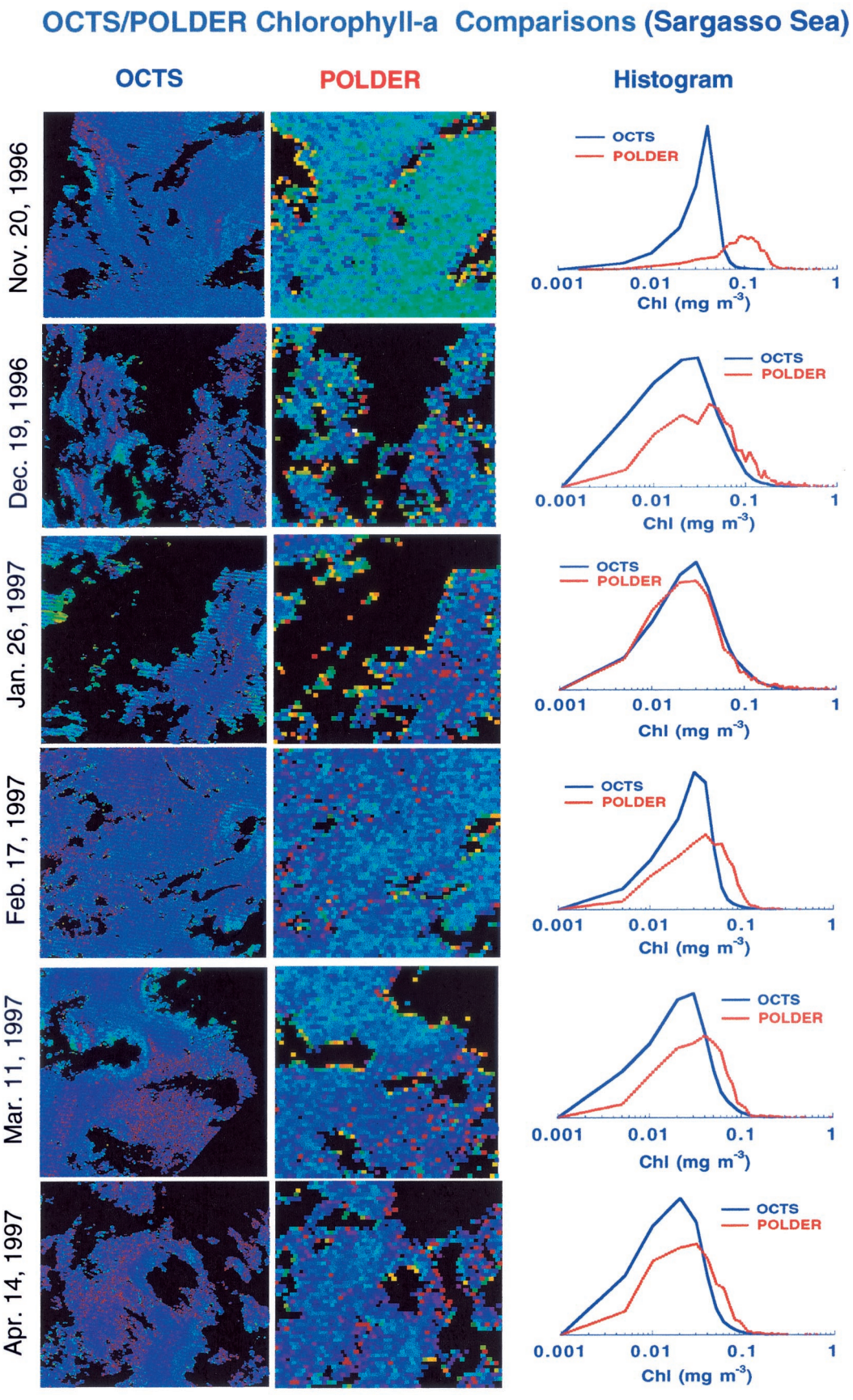

Fig. 9. OCTS-retrieved chlorophyll a concentration compared with those derived from POLDER measurements for the Sargasso Sea from Nov. 20, 1996 to April 14, 1997. The color scale is indicated at the bottom of Fig. 10.

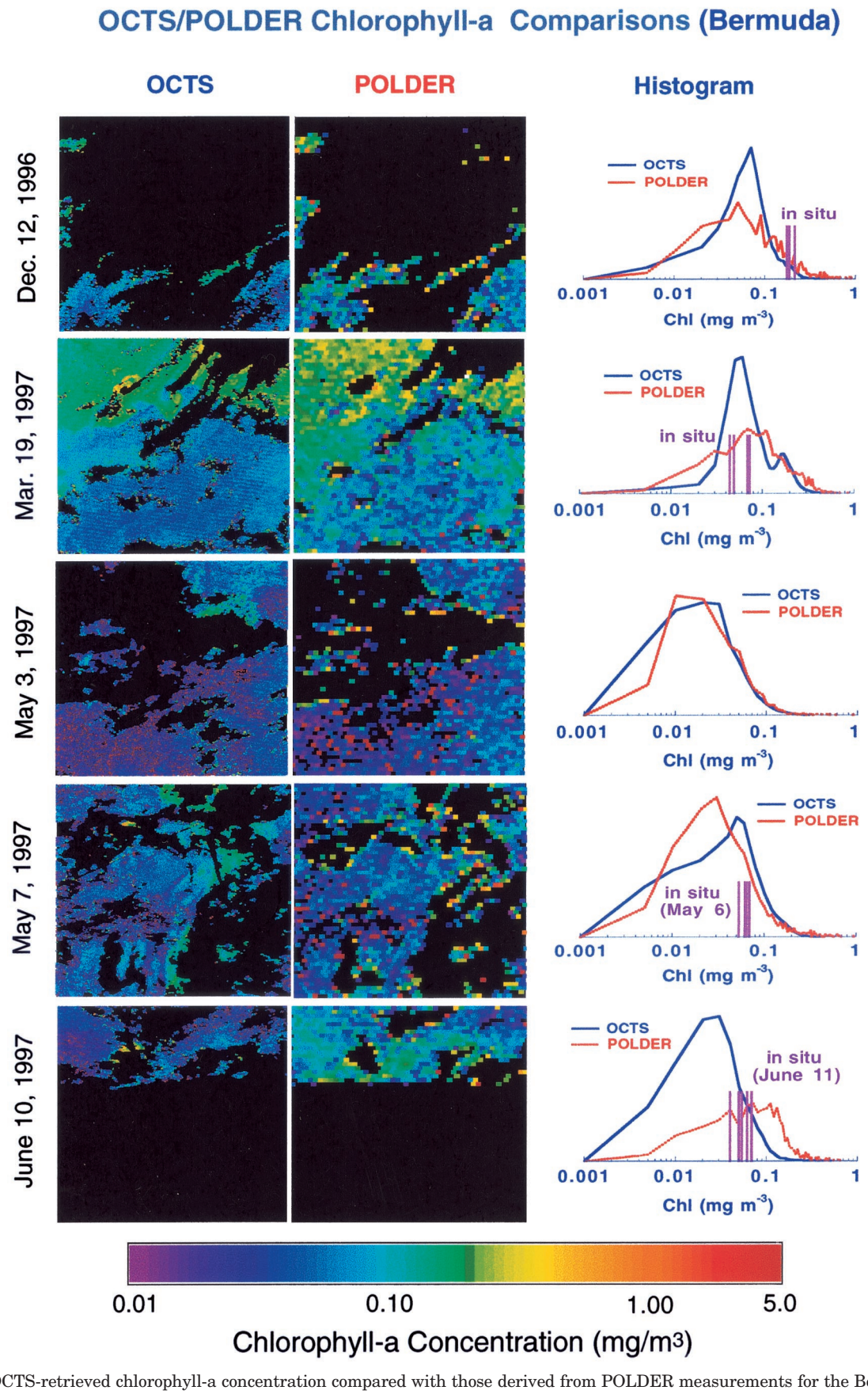

Fig. 10. OCTS-retrieved chlorophyll-a concentration compared with those derived from POLDER measurements for the Bermuda area from Dec. 12, 1996 to June 10, 1997. Some of the *in situ* measurements, which were acquired at the location near the center of the images, are also indicated as vertical bars in the histograms over the Bermuda area.

the *in situ* measurements. The same is also true for the case of June 10, 1997, where there were no retrievals for the bottom-most two-thirds part of the images. On the other hand, when coverage did coincide with field data as for both March 19, 1997 and May 7, 1997 both satellite data compared well with *in situ* measurements. Note that *in situ* data for May 7, 1997 and June 10, 1997 were obtained one day earlier (May 6, 1997) and one day later (June 11, 1997), respectively.

There are obvious variations in the derived chlorophyll-a concentrations between OCTS and POLDER. However, it is found that, for the chlorophyll-a concentration comparison, the overall average ratio value (mode in histogram) of OCTS/POLDER for all the Sargasso Sea and the Bermuda area cases (total of 12) is 0.9907 with a relative large standard deviation of 0.4817.

D. Discussion

According to the results of the comparisons between OCTS and POLDER, it is clear that there are no obvious bias differences in the derived products between the two sensors. However, it has been consistently shown that, compared to OCTS, the POLDER-derived ocean-color data are often more noisy, in particular, for data derived from the POLDER 443-nm band (see results in Figs. 7 and 8). One possible reason for such variability could be due to POLDER sensor nonlinearity.[37] Results have shown[37] that the POLDER sensor nonlinear responses underestimate radiance values at the lower radiance ranges and overestimate values for the high radiance ranges. It was reported[37] that the POLDER 443-nm band has a ~3% nonlinear variation from low to high radiances for ocean-color measurements. Other bands also have nonlinear responses, but with much smaller magnitudes.[37]

Some high sparkling values in the POLDER-derived ocean color products, however, are mostly from the cloud-edge effects, owing to subpixel cloud contamination. With a low-spatial-resolution pixel, POLDER measurements are more likely to be contaminated by subpixel clouds. The cloud contaminated pixels could be misidentified as clear because their radiance values are not high enough to trigger the cloud threshold.

6. Conclusion

We describe a procedure to calibrate vicariously OCTS and POLDER Level-1B data using the MOBY *in situ* measurements. This procedure effectively bridges the OCTS and POLDER Level-1B data through the use of a common set of MOBY *in situ* measurements. The vicarious calibration assumes the band 865-nm gain coefficients are not changed, while the visible bands are adjusted such that the derived normalized water-leaving radiances are forced to be equivalent to the MOBY *in situ* measurements. Using the derived gain coefficients, we can use a consistent atmospheric-correction algorithm to process OCTS and POLDER data from Level-1B to Level-2 products. Therefore the differences in the OCTS and POLDER-derived ocean-color products are mainly from the differences of the sensor characteristics, i.e., with this approach, the retrieved products would be identical if the two sensors were identical.

We demonstrate the efficacy of vicariously recalibrating OCTS and POLDER with a common *in situ* data set and using a consistent atmospheric-correction algorithm for data processing. Both the OCTS- and POLDER-derived normalized water-leaving radiances compare reasonably well with independent *in situ* data. Over the Sargasso Sea and the Bermuda area, the ocean-color products derived from OCTS have a good agreement with data from POLDER measurements. It is particularly important that there are no obvious bias differences between the OCTS- and POLDER-derived ocean-color data, i.e., the overall ratio values between the OCTS- and POLDER-derived normalized water-leaving radiances at 443, 490, and 565 nm are 1.0004, 1.0103, and 0.9840, while the ratio value in the derived chlorophyll-a concentration is 0.9907. However, the noise differences, which are usually inherited from sensor characteristics, are difficult to remove at the pixel level. These noise differences possibly can be reduced with data-averaging schemes (e.g., averaging Level-2 data to Level-3 products). To resolve the noise problem, however, one will generally need improved instruments, e.g., high sensor signal-to-noise performance, good sensor linearity response, and high radiometric stability. It is found that the POLDER-derived $[L_w(\lambda)]_N$ are usually more noisy than those of OCTS, in particular, for the 443-nm band products. This most likely results from the POLDER sensor nonlinearity response problem.[37] On the other hand, effects of the subpixel cloud contamination around cloud edge lead to high sparkling values in the POLDER-retrieved ocean color products.

The OCTS and POLDER data-processing procedures and algorithms are scheduled to be implemented in MSL12 within the SeaDAS software,[12] which is freely available. Therefore interested scientists can process OCTS and POLDER data with the widely distributed SeaDAS software package.

The OCTS and POLDER Level-1B data were provided by National Space Development Agency of Japan and Centre National d'Etudes Spatioles of France. We thank J.-M. Nicolas for his assistance with the POLDER Level-1B data, D. Clark and his research group for providing the MOBY data, J. O'Reilly and S. Maritorena for the modified OC2 algorithm, F. Patt for help in OCTS navigation analyses, S. Bailey and J. Werdell for help for the SeaBASS *in situ* data analyses, and two anonymous reviewers for their helpful comments. This research was supported by funding provided by National Aeronautics and Space Administration under the Sensor Intercomparison and Merger for Biological and Interdisciplinary Oceanic Studies (SIMBIOS) project and partly from NASA SIMBIOS grant NAS5-00203.

References

1. J. Tanii, T. Machida, H. Ayada, Y. Katsuyama, J. Ishida, N. Iwasaki, Y. Tange, Y. Miyachi and R. Sato, "Ocean Color and Temperature Scanner (OCTS) for ADEOS," in *Future European and Japanese Remote-Sensing Sensors and Programs: Proceedings of the Meeting, Orlando, Fla, April 1, 2, 1991*, P. N. Slater, ed. Proc. SPIE **1490,** 200–206 (1991).
2. P. Y. Deschamps, F. M. Bréon, M. Leroy, A. Podaire, A. Bricaud, J. C. Buriez and G. Sèze, "The POLDER mission: instrument characteristics and scientific objectives," IEEE Trans. Geosci. Remote Sens. **32,** 598–615 (1994).
3. C. R. McClain and G. S. Fargion, "SIMBIOS Project 1999 Annual Report," SIMBIOS Technical Report Series, NASA Tech. Memo. 1999-209486 (NASA Goddard Space Flight Center, Greenbelt, Md., 1999).
4. M. Wang and B. A. Franz, "Comparing the ocean color measurements between MOS and SeaWiFS: a vicarious intercalibration approach for MOS," IEEE Trans. Geosci. Remote Sens. **38,** 184–197 (2000).
5. G. Zimmermann and A. Neumann, "The Spaceborne imaging spectrometer MOS for ocean remote sensing," in *Proceedings of the 1st International Workshop on MOS-IRS and Ocean Color, Berlin, April 28–30* (Institute of Space Sensor Technology, German Aerospace Center, Berlin, 1997), pp. 1–9.
6. S. B. Hooker, W. E. Esaias, G. C. Feldman, W. W. Gregg and C. R. McClain, *An Overview of SeaWiFS and Ocean Color*, Vol. 1 of SeaWiFS Technical Report Series, NASA Tech. Memo. 104566, S. B. Hooker and E. R. Firestone, eds. (NASA Goddard Space Flight Center, Greenbelt, Md., 1992).
7. C. R. McClain, M. L. Cleave, G. C. Feldman, W. W. Gregg, S. B. Hooker and N. Kuring, "Science quality SeaWiFS data for global biosphere research," Sea Technol. **39,** 10–16 (1998).
8. D. K. Clark, H. R. Gordon, K. J. Voss, Y. Ge, W. Broenkow, and C. Trees, "Validation of atmospheric correction over the ocean," J. Geophys. Res. **102,** 17209–17217 (1997).
9. H. R. Gordon and M. Wang, "Retrieval of water-leaving radiance and aerosol optical thickness over the oceans with SeaWiFS: a preliminary algorithm," Appl. Opt. **33,** 443–452 (1994).
10. H. Fukushima, A. Higurashi, Y. Mitomi, T. Nakajima, T. Noguchi, T. Tanaka, and M. Toratani, "Correction of atmospheric effects on ADEOS/OCTS ocean color data: algorithm description and evaluation of its performance," J. Oceanogr. **54,** 417–430 (1998).
11. H. R. Gordon, "Atmospheric correction of ocean color imagery in the Earth Observing System era," J. Geophys. Res. **102,** 17081–17106 (1997).
12. K. Baith, R. Lindsay, G. Fu and C. R. McClain, "Data analysis system developed for ocean color satellite sensors," Eos Trans. Am. Geophys. Union **82** (Eos electronic supplement: http://www.agu.org/eos_elec/00289e.html, May 1, 2001).
13. W. W. Gregg, "Initial analysis of ocean color data from the ocean color and temperature scanner. I. Imagery analysis," Appl. Opt. **38,** 476–485 (1999).
14. M. Shimada, H. Oaku, Y. Mitomi, H. Murakami, Y. Nakamura, J. Ishizaka, H. Kawamura, T. Tanaka, M. Kishino and H. Fukushima, "Calibration and validation of the ocean color version-3 product from ADEOS OCTS," J. Oceanogr. **54,** 401–416 (1998).
15. F. S. Patt and W. W. Gregg, "Exact closed-form geolocation algorithm for earth survey sensors," Int. J. Remote Sens. **15,** 3719–3734 (1994).
16. F. S. Patt, R. H. Woodward and W. W. Gregg, "An automated method for navigation assessment for Earth survey sensors using island targets," Int. J. Remote Sens. **18,** 3311–3336 (1997).
17. H. R. Gordon and M. Wang, "Influence of oceanic whitecaps on atmospheric correction of ocean-color sensor," Appl. Opt. **33,** 7754–7763 (1994).
18. D. Antoine and A. Morel, "A multiple scattering algorithm for atmospheric correction of remotely sensed ocean colour (MERIS instrument): principle and implementation for atmospheres carrying various aerosols including absorbing ones," Int. J. Remote Sens. **20,** 1875–1916 (1999).
19. H. Yang and H. R. Gordon, "Remote sensing of ocean color: assessment of water-leaving radiance bidirectional effects on atmospheric diffuse transmittance," Appl. Opt. **36,** 7887–7897 (1997).
20. M. Wang, "Atmospheric correction of ocean color sensors: computing atmospheric diffuse transmittance," Appl. Opt. **38,** 451–455 (1999).
21. H. R. Gordon, O. B. Brown, R. H. Evans, J. W. Brown, R. C. Smith, K. S. Baker and D. K. Clark, "A semianalytic radiance model of ocean color," J. Geophys. Res. **93,** 10909–10924 (1988).
22. A. Morel, "Optical modeling of the upper ocean in relation to its biogenous matter content (case 1 waters)," J. Geophys. Res. **93,** 10749–10768 (1988).
23. J. E. O'Reilly, S. Maritorena, B. G. Mitchell, D. A. Siegel, K. L. Carder, S. A. Garver, M. Kahru and C. R. McClain, "Ocean color chlorophyll algorithms for SeaWiFS," J. Geophys. Res. **103,** 24937–24953 (1998).
24. M. Wang, "A sensitivity study of SeaWiFS atmospheric correction algorithm: Effects of spectral band variations," Remote Sens. Environ. **67,** 348–359 (1999).
25. K. Ding and H. R. Gordon, "Analysis of the influence of O_2 A-band absorption on atmospheric correction of ocean color imagery," Appl. Opt. **34,** 2068–2080 (1995).
26. M. Wang, "Validation study of the SeaWiFS oxygen A-band absorption correction: comparing the retrieved cloud optical thicknesses from SeaWiFS measurements," Appl. Opt. **38,** 937–944 (1999).
27. M. Wang, "The SeaWiFS atmospheric correction algorithm updates," Vol. 9 of SeaWiFS Postlaunch Technical Report Series, NASA Tech. Memo. 2000-206892, S. B. Hooker and E. R. Firestone, eds. (NASA Goddard Space Flight Center, Greenbelt, Md., 2000).
28. D. A. Siegel, M. Wang, S. Maritorena and W. Robinson, "Atmospheric correction of satellite ocean color imagery: the black pixel assumption," Appl. Opt. **39,** 3582–3591 (2000).
29. H. R. Gordon and M. Wang, "Surface roughness considerations for atmospheric correction of ocean color sensors. 1. the Rayleigh scattering component," Appl. Opt. **31,** 4247–4260 (1992).
30. M. Wang, "The Rayleigh lookup tables for the SeaWiFS data processing: including effects of ocean surface roughness," Int. J. Remote Sens. (to be published).
31. M. Wang and S. Bailey, "Correction of the sun glint contamination on the SeaWiFS ocean and atmosphere products," Appl. Opt. **40,** 4790–4798.
32. R. Frouin, M. Schwindling, and P. Y. Deschamps, "Spectral reflectance of sea foam in the visible and near infrared: in situ measurements and remote sensing implications," J. Geophys. Res. **101,** 14361–14371 (1996).
33. K. D. Moore, K. J. Voss, and H. R. Gordon, "Spectral reflectance of whitecaps: instrumentation, calibration, and performance in coastal waters," J. Atmos. Ocean. Tech. **15,** 496–509 (1998).
34. K. D. Moore, K. J. Voss, and H. R. Gordon, "Spectral reflectance of whitecaps: their contribution to water-leaving radiance," J. Geophys. Res. **105,** 6493–6499 (2000).
35. E. P. Shettle and R. W. Fenn, "Models for the aerosols of the lower atmosphere and the effects of humidity variations on their optical properties," AFGL-TR-79-0214, (U.S. Air Force Geophysics Laboratory, Hanscom Air Force Base, Mass., 1979).
36. M. Wang, B. A. Franz, R. A. Barnes and C. R. McClain, "Effects

of spectral bandpass on SeaWiFS-retrieved near-surface optical properties of the ocean," Appl. Opt. **40,** 342–348 (2001).
37. B. Fougnie, O. Hagolle, and F. Cabot, "In-flight measurement and correction of nonlinearity of the POLDER-1's sensitivity," in *Proceedings of Physical Measurements and Signatures in Remote Sensing, Aussois, France, January 8–12, 2001* (International Society for Photogrammetry and Remote Sensing, Amsterdam, The Netherlands, 2001), pp. 211–219.
38. H. R. Gordon, "In-orbit calibration strategy for ocean color sensors," Remote Sens. Environ. **63,** 265–278 (1998).
39. W. Robinson and M. Wang, "Vicarious calibration of the SeaWiFS band 7," Vol 9 of SeaWiFS Postlaunch Technical Report Series, NASA Tech. Memo. 2000-206892, S. B. Hooker and E. R. Firestone, eds. (NASA Goddard Space Flight Center, Greenbelt, Md., 2000).
40. R. E. Eplee and C. R. McClain, "MOBY Data Analysis for the Vicarious Calibration of SeaWiFS Bands 1-6," Vol. 9 of SeaWiFS Postlaunch Technical Report Series, NASA Tech. Memo. 2000-206892, S. B. Hooker and E. R. Firestone, eds. (NASA Goddard Space Flight Center, Greenbelt, Md., 2000).
41. O. Hagolle, P. Goloub, P. Y. Deschamps, H. Cosnefroy, X. Briottet, T. Bailleul, J. M. Nicolas, F. Parol, B. Lafrance and M. Herman, "Results of POLDER in-flight calibration," IEEE Trans. Geosci. Remote Sens. **37,** 1550–1566 (1999).